

Surface plasmon dispersion of semiconductors with depletion or accumulation layers

Cheng C. Kao* and Esther M. Conwell

Xerox Webster Research Center, Rochester, New York 14644

(Received 15 March 1976)

We have calculated the effect on the surface-plasmon-polariton dispersion of a space-charge layer at a semiconductor surface, representing it by a dielectric function $\epsilon(\omega)$ that has an exponentially varying part with a $1/e$ decay depth of the order of the layer thickness. Since we are interested in frequencies below those where interband transitions are important, we have used a free-electron model for $\epsilon(\omega)$, with the plasma frequency varying continuously from ω_{ps} at the surface to ω_{pb} in the bulk. Particular attention has been paid to the frequency range for which the real part of ϵ vanishes within the sample. Use of a local relation between dielectric displacement and electric field is justified, even in this range, by the fact that we use complex ϵ and the imaginary part varies little with depth. Evaluating the dispersion numerically, with damping included, we obtain for the dispersion of a depletion layer ($\omega_{ps} < \omega_{pb}$) a single branch that starts at the light line, is reentrant at ω_{ps} , and goes asymptotically to the frequency for which ϵ at the surface ϵ_s equals $-\epsilon$ of the medium above. For samples with thick enough depletion layers, additional branches, corresponding to guided modes, are found both above and below ω_{pb} . For an accumulation layer ($\omega_{ps} > \omega_{pb}$) there is always one branch which starts at the light line and goes asymptotically to the frequency for which $\epsilon_s = -\epsilon$ of the medium above. For large enough values of d , a second branch appears, lying between ω_{pb} and ω_{ps} , curving upward in contradiction to results obtained earlier. Comparison of this theory with experimental data for InSb, some for samples with disturbed surfaces, leads to reasonable estimates for the thickness of the surface depletion layers.

I. INTRODUCTION

Measurements of surface-plasmon-polariton (SPP) dispersion, made on n -InSb,¹⁻³ indicate that the space-charge region at the surface of a semiconductor does have an effect on the dispersion. Attempts to calculate this effect have been made by a number of investigators. In an early calculation, Wallis *et al.*⁴ replaced the space-charge region by a thin uniform layer with fewer or more carriers than the bulk to represent a depletion or accumulation layer, respectively. Cunningham *et al.*⁵ took into account the variation of the dielectric constant ϵ within the sample by replacing ϵ with a piecewise-continuous function. One or more linearly varying regions of ϵ were joined onto one or more regions of constant ϵ to simulate various types of space-charge variation with depth. Rice *et al.*,^{6,7} although more interested in the effect of accumulation or depletion layers on metals, approximated ϵ by

$$\epsilon(\omega; z) = \epsilon_b(\omega) + \Delta\epsilon(\omega)e^{z/d}, \quad z < 0 \quad (1.1)$$

where z is the depth below the surface, taken as $z=0$, and d a parameter of the order of the space-charge region width. Solving the wave equation using (1.1), they concluded that the presence of either a depletion or accumulation layer leads to an extra branch in the dispersion. As pointed out by them, this could provide a useful tool for the study of surfaces. However, one of us subsequently showed,^{8,9} using (1.1), that the extra branch found by them could not exist for the case $|\Delta\epsilon/\epsilon|$

$\ll 1$. It remained a question whether extra branches could exist for large $|\Delta\epsilon/\epsilon|$, in particular, for the case where ϵ goes through 0 within the sample. With the calculations to be described below, we have now concluded that for that case extra branches can exist, both for accumulation and depletion layers, but they have different properties from those found by Rice *et al.* In the case of depletion layers, where the extra branches are more properly described as guided modes,¹⁰ they require larger values of d (or, more accurately, of the product of d and the plasma frequency) than were considered by Rice *et al.*

In Sec. II we give a more complete statement of the problem and our approach to solving it. We are again using (1.1) for ϵ but, as will be seen, solution of the wave equation becomes much more difficult when the region where ϵ vanishes is included. The use of (1.1) implies a local relation between \vec{D} and \vec{E} , which is questionable particularly in the neighborhood of $\epsilon = 0$. In Sec. II we show that the local relation is valid provided complex ϵ is used. ϵ is taken from a free-electron model, known to be a good approximation at frequencies below E_g/h , where E_g is the energy gap, in InSb and GaAs, for example. Having set up the wave equation for TM modes in an inhomogeneous medium in Sec. II, we proceed to solve it in Sec. III. Solution for all $z < 0$, for ω 's above and below the bulk-plasma frequency and for either depletion or accumulation layers, requires three series expansions, two about the singular points and the third at the surface, which is generally a regular point. One con-

stant of integration is obtained by use of the boundary condition at $z = -\infty$. The other, of course, remains arbitrary, determined by the input power. Under some conditions only one series solution is needed to cover the entire region $z < 0$, but more often two or even three series solutions must be used, properly joined, to construct a general solution. The details of this and the resulting dispersion relations, obtained by requiring the continuity of tangential \vec{E} and \vec{H} at $z = 0$, are presented in Sec. IV. The results thus obtained are concise in form, but the dispersion can only be obtained by computer. In Sec. V we give numerical results for the dispersion and field variation with depth for a number of representative depletion layer cases. At first ϵ is assumed to be real and then the effects of moderate damping are considered. We also compare our theory with the available experimental results. The final section (Sec. VI) is devoted to representative results for accumulation layers.

II. STATEMENT OF PROBLEM

A local relation between \vec{D} and \vec{E} was used in all the calculations referred to earlier.⁴⁻¹⁰ Its validity is discussed at length by Cunningham, Maradudin, and Wallis (CMW),⁵ who show that it is questionable only in regions where carrier concentration or electric field vary rapidly with z over a distance comparable to the screening length. Certainly in a region where ϵ goes through 0, resulting in the electric field becoming infinite, a local approximation cannot be justified. Although CMW can show that its use leads to correct results for one particular (limiting) case which can be solved without this approximation, ultimately they justify its use overall by noting that it leads to generally reasonable dispersion. Since the dispersion depends on the field everywhere, the fact that the fields are incorrect in a small volume due to use of this approximation, they reason, should have little effect on the dispersion. This reasoning should be satisfactory if the region in which the field divergence occurs is not close to $z = 0$, where the continuity conditions are applied to determine the dispersion relation. As will be seen, however, when we temporarily assume ϵ real and evaluate the dispersion for frequencies at which $\epsilon = 0$ is close to the surface, the local approximation leads to spurious results. We can avoid this by taking into account damping.

On a free-electron model,¹¹ for frequencies such that the mean carrier scattering time $\tau \gg 1/\omega$,

$$\epsilon(\omega) = \epsilon_\infty(1 - \omega_p^2\omega^{-2}) + i\epsilon_\infty(\omega_p^2\omega^{-2})(\omega\tau)^{-1}, \quad (2.1)$$

where ϵ_∞ is the dielectric constant at high frequencies (but not so high that interband transitions

contribute to ϵ) and ω_p is the plasma frequency. If the carrier concentration N varies slowly with z , as is true in the cases of our interest, we may define a local plasma frequency

$$\omega_p^2(z) = 4\pi N(z)e^2/\epsilon_\infty m^*(z), \quad (2.2)$$

where e and m^* are the charge and effective mass of the carriers, respectively. When the carrier concentration varies with z , τ may vary with z , although not as strongly as ω_p^2 does. Of course, for a damaged surface, where other defects are introduced, τ might vary strongly with z but we shall not consider such cases quantitatively. Thus for the cases we do treat, ϵ_I , the imaginary part of ϵ , is both slowly varying with z and large enough, as will be seen, so that the electric field rises less than an order of magnitude in the neighborhood where ϵ_R , the real part of ϵ , vanishes. Thus even in that neighborhood the assumption of a local relation between \vec{D} and \vec{E} should be satisfactory provided complex ϵ is used. In what follows we use complex ϵ unless otherwise specified.

The medium in the upper half-space ($z > 0$) is assumed homogeneous with a dielectric constant ϵ_2 independent of frequency and position. We look for solutions representing plane electromagnetic waves propagating along the x direction with wave vector k_x . For the symmetry of the system we are discussing, electromagnetic wave propagation can be split into TM and TE modes. In this paper we shall be concerned only with TM modes. TE modes in this frequency range are found also to have some special properties, which have been discussed in another publication.¹² For TM modes the amplitudes of the three field components may be taken H_y , E_x , and E_z . To obtain the fields, each amplitude must be multiplied by $\exp[i(k_x x - \omega t)]$. The magnetic field amplitude then satisfies the following wave equation¹³:

$$\frac{d}{dz} \left(\frac{1}{\epsilon} \frac{dH_y}{dz} \right) + \left(\frac{\omega^2}{c^2} - \frac{k_x^2}{\epsilon} \right) H_y = 0, \quad (2.3)$$

with c denoting the velocity of light in free space. The electric fields E_x and E_z may be obtained from

$$E_x = \frac{1}{i\omega\epsilon} \frac{dH_y}{dz}, \quad (2.4)$$

$$E_z = -(k_x/\omega\epsilon)H_y. \quad (2.5)$$

In Sec. III our efforts will be directed to solution of Eq. (2.3) with $\epsilon = \epsilon_2$ for $z > 0$, ϵ given by (1.1) for $z < 0$. The location z_0 where the real part of ϵ vanishes is given by

$$z_0 = d \ln[(\omega_{pb}^2 - \omega^2)/(\omega_{pb}^2 - \omega_{ps}^2)], \quad (2.6)$$

where ω_{pb} and ω_{ps} are the bulk and surface values of the plasma frequency, respectively,

III. SOLUTIONS OF TM-MODE WAVE EQUATION

Since $\epsilon = \epsilon_2$, independent of z , for $z > 0$, the wave equation in the upper half-space is easily solved. The solution that is finite as $z \rightarrow \infty$ is

$$H_y(z) = H_{ys} \exp(-p_2 z), \quad z > 0 \tag{3.1}$$

with

$$p_2 = (k_x^2 - \epsilon_2 \omega^2 c^{-2})^{1/2}. \tag{3.2}$$

Here H_{ys} denotes the value at $z = 0$. Since the parameter p_2 must be real and positive, the lower bound of k_x is the light line, given by $k_x = \sqrt{\epsilon_2} \omega / c$.

In the lower half-space, the situation is much more complicated because of the z dependence of ϵ given in (1.1). However, since $\epsilon \rightarrow \epsilon_b$ as $z \rightarrow -\infty$, the wave equation in that limit approaches that of the upper half-space with ϵ_b replacing ϵ_2 . Then

$$\lim_{z \rightarrow -\infty} H_y = (\text{const}) \exp(p_0 z), \tag{3.3}$$

with

$$p_0 = (k_x^2 - \epsilon_b \omega^2 c^{-2})^{1/2}. \tag{3.4}$$

The general solution may therefore be expressed by

$$H_y(z) = F(z) \exp(p_0 z), \quad z < 0. \tag{3.5}$$

The unknown function $F(z)$ must approach a constant as $z \rightarrow -\infty$. Introducing a new variable

$$v = -\epsilon(z) / \epsilon_b, \tag{3.6}$$

we can transform the wave equation for $z < 0$ into the differential equation

$$v(v+1)F'' + (2\alpha v - 1)F' - (\alpha + qv)F = 0, \tag{3.7}$$

where the prime indicates d/dv and

$$\alpha = p_0 d, \tag{3.8}$$

$$q = \epsilon_b \omega^2 d^2 / c^2. \tag{3.9}$$

In what follows we shall make considerable use of the surface value of v , v_s , given by

$$v_s = -\epsilon_s / \epsilon_b. \tag{3.10}$$

The surface dielectric constant ϵ_s is related to ϵ_b by

$$\epsilon_s = \epsilon_b + \Delta\epsilon. \tag{3.11}$$

Consider now the behavior of the above differential equation in the complex v space. There are two regular singular points, one at $v = 0$ where $\epsilon = 0$ and the other at $v = -1$ where $z \rightarrow -\infty$. The region at infinity (i.e., $|v| \rightarrow \infty$) forms an essential singularity if $\epsilon_b \neq 0$. All other points in v space are ordinary points. Standard Frobenius methods¹⁴ can be applied to solve this kind of differential equation in terms of infinite series expanded at regular singular or ordinary points. A series thus obtained is valid only within a radius of convergence equal to the distance from the expansion point to the nearest singularity. If several such series can be found and properly combined a complete solution covering the entire region of interest can always be obtained. In the present case, we are mainly interested in a strip including the entire real axis of the complex v space. In the following we shall present the three solutions needed: one expanded about $v = 0$, a second about $v = -1$, and a third about $v = v_s \neq 0, -1$.

A. Series solution expanded about the singular point $v = 0$

The series solution given in this subsection will be called the v solution. Since $v = 0$ occurs if $\epsilon = 0$, this solution is particularly useful if the real part of the dielectric constant crosses zero somewhere inside the medium. This happens for ω 's between the bulk-plasma frequency ω_{pb} and the surface-plasma frequency ω_{ps} . Using Frobenius methods in this case, we find that the function F can be expressed as

$$F = A_v F_v, \tag{3.12}$$

with

$$F_v = g F_a + F_b. \tag{3.13}$$

Here A_v and g are two unknown integration constants, and F_a and F_b are infinite series given by

$$F_a = \sum_{n=0}^{\infty} a_n v^n, \tag{3.14}$$

$$F_b = \frac{1}{2}(q + \alpha^2) (\ln v) F_a + \sum_{n=0}^{\infty} b_n v^n, \tag{3.15}$$

with the following coefficients

$$a_0 = a_1 = 0, \quad a_2 = 1, \tag{3.16}$$

$$a_n = -[n(n-2)]^{-1} \{ [n(n-1)(n-2) + \alpha(2n-3)] a_{n-1} - q a_{n-2} \} \equiv M_1(a_{n-1}, a_{n-2}), \quad n \geq 3$$

$$b_0 = 1, \quad b_1 = -\alpha, \quad b_2 = -(q - 4\alpha + \alpha^2) / 4, \tag{3.17}$$

$$b_n = M_1(b_{n-1}, b_{n-2}) - (q + \alpha^2) [2n(n-2)]^{-1} [2(n-1)a_n + (2n-3+2\alpha)a_{n-1}], \quad n \geq 3.$$

For real v , the function $\ln v$ in (3.15) is replaced by $\ln|v|$.

B. Series solution expanded about the singular point $v=-1$

Since $v=-1$ occurs as $z \rightarrow -\infty$, the series solution expanded at $v=-1$ is particularly useful when the solution deep in the bulk is needed. For convenience, we write (3.7) in terms of a new variable y defined by

$$y = v + 1. \quad (3.18)$$

The solution of this equation, obtained earlier in Ref. 6, will be called the y solution. It may be written

$$F = A_y F_y, \quad (3.19)$$

where A_y is an integration constant and the infinite series F_y is given by

$$F_y = \sum_{n=0}^{\infty} c_n y^n, \quad (3.20)$$

with the following coefficients

$$\begin{aligned} c_{-1} = 0, c_0 = 1, \\ c_n = [n(n+2\alpha)]^{-1} \{ (n-1)(n-2) \\ + \alpha(2n-3) + q \} [c_{n-1} - qc_{n-2}], \quad n \geq 1. \end{aligned} \quad (3.21)$$

C. Series solution expanded about an ordinary point $v=v_s \neq 0, -1$

Suppose $v_s \neq 0$ or -1 . The point $v=v_s$ then an ordinary point of the differential equation. For convenience, let us define a new variable u by

$$u = (v - v_s)/R, \quad (3.22)$$

with

$$R = \begin{cases} -v_s - 1, & \text{if } v_s \leq -\frac{1}{2}. \\ -v_s, & \text{if } v_s \geq -\frac{1}{2}. \end{cases} \quad (3.23)$$

The solution to be given next will be called the u solution, and $|R|$ is its radius of convergence. In this case we find that the function F can be written as

$$F = A_u F_u, \quad (3.24)$$

with

$$F_u = F_d + h F_e. \quad (3.25)$$

Here A_u and h are integration constants, and F_d and F_e infinite series given by

$$F_d = \sum_{n=0}^{\infty} d_n u^n, \quad (3.26)$$

$$F_e = \sum_{n=0}^{\infty} e_n u^n, \quad (3.27)$$

with the following coefficients:

$$\begin{aligned} d_{-1} = 0, d_0 = 1, d_1 = 0, \\ d_n = -R^2 [v_s(v_s+1)n(n-1)]^{-1} \\ \times \{ R^{-1}(n-1)[(2v_s+1)(n-2) + 2\alpha v_s - 1] d_{n-1} \\ + [(n-2)(n-3+2\alpha) - qv_s - \alpha] d_{n-2} - qR d_{n-3} \}, \\ \equiv M_2(d_{n-1}, d_{n-2}, d_{n-3}), \quad n \geq 2 \\ e_{-1} = e_0 = 0, e_1 = 1, \\ e_n = M_2(e_{n-1}, e_{n-2}, e_{n-3}), \quad n \geq 2 \end{aligned} \quad (3.28)$$

Since this u solution is expanded about $v=v_s$, it is most useful near the surface.

Each of the above three solutions, v , y , or u , has its own unique region of convergence. Table I summarizes the various ranges of convergence on the real axis of the complex v space for the three solutions, first in terms of the variable v , then in terms of the dielectric constant ϵ , and lastly in terms of the depth z . Under certain conditions either the v or y solution alone can be used for the whole inhomogeneous medium. In terms of the frequency ω , we have summarized these conditions in Table II. Note that different frequency ranges need to be considered depending on the relative values of ω_{ps} and ω_{pb} .

IV. INTEGRATION CONSTANTS AND DISPERSION RELATIONS

The integration constants (g, h, A_v, A_y , and A_u) in the series solutions presented in the Sec. III must be determined by appropriate boundary conditions. As has been discussed above, sometimes only one solution is needed for all $z < 0$. In such cases, only the boundary conditions at the surface and deep in the bulk are needed to determine the unknown constants. The requirement at the surface is that the tangential electric and magnetic fields be continuous, and deep in the bulk the fields must remain finite.¹⁵ However, in cases that two or three solutions are needed to cover $z < 0$, additional boundaries (not real in the sense of bounding two different media) have to be chosen, one in each overlap region between two neighboring solutions, and field continuity established there. The value of v at the surface, v_s , determines the solutions required or convenient to use. This information is summarized in Table III. For all cases we have found that the dispersion relation can be written in a general form in terms of the solution evaluated at the surface as

TABLE I. Ranges of convergence for the series solutions v , y , and u (ϵ real).

Series solution	Definition of variable	Ranges of convergence in terms of		
		v	ϵ	z
v	$-\epsilon/\epsilon_b$	$ v < 1$	$ \epsilon < \epsilon_b $	$z < 0$ if $ v_s < 1$ or $ \epsilon_s/\epsilon_b < 1$. $z < d \ln(-2\epsilon_b/\Delta\epsilon)$ if $v_s \geq 1$ or $\epsilon_s/\epsilon_b \leq -1$. Not valid if $v_s \leq -1$ or $\epsilon_s/\epsilon_b \geq 1$.
y	$v+1$	$-2 < v < 0$	$ \epsilon - \epsilon_b < \epsilon_b $	$z < 0$ if $-2 < v_s < 0$ or $ \Delta\epsilon < \epsilon_b $. $z < d \ln \epsilon_b/\Delta\epsilon $ if $ \Delta\epsilon \geq \epsilon_b $.
u	$(v - v_s)/R$ $R = -v_s - 1$, if $v_s \leq -\frac{1}{2}$. $R = -v_s$, if $v_s \geq -\frac{1}{2}$. $(v_s \neq 0, -1)$	$ v - v_s < R $	$ \epsilon - \epsilon_s < \Delta\epsilon $ if $v_s \leq -\frac{1}{2}$ $ \epsilon - \epsilon_s < \epsilon_s $, if $v_s \geq -\frac{1}{2}$	$z < 0$ if $v_s \leq -\frac{1}{2}$. $0 > z > d \ln(1 - \epsilon_s/\Delta\epsilon)$ if $v_s \geq -\frac{1}{2}$

$$\frac{\beta}{\epsilon_2} = -\frac{\alpha}{\epsilon_s} \left[1 + \frac{v_s + 1}{\alpha} \left(\frac{F'}{F} \right)_{z=0} \right], \tag{4.1}$$

where the prime indicates d/dv and

$$\beta = p_2 d. \tag{4.2}$$

In what follows we shall study first those cases where either the v or y solution can be used alone, and then discuss situations in which multiple solutions must be matched.

A. Use of v solution alone for $|v_s| < 1$

As shown in Table I, the v solution alone can be used for all $z < 0$ if $|v_s| < 1$, with the applicable frequency ranges given in Table II. The unknown constant g can be determined by the condition that, as

TABLE II. Frequency ranges in which v or y solution is valid for all $z < 0$.

Series solution	Depletion layer $\omega_{ps} < \omega_{pb}$	Accumulation layer $\omega_{ps} > \omega_{pb}$
v	$\omega < [(\omega_{pb}^2 + \omega_{ps}^2)/2]^{1/2}$	$\omega > [(\omega_{pb}^2 + \omega_{ps}^2)/2]^{1/2}$
y	$\omega < \omega_{ps}$, or $\omega > (2\omega_{pb}^2 - \omega_{ps}^2)^{1/2}$	$\omega > \omega_{ps}$, or $\omega < (2\omega_{pb}^2 - \omega_{ps}^2)^{1/2}$, if $\omega_{pb} > \omega_{ps}/\sqrt{2}$

noted earlier, $F \rightarrow \text{const}$ as $z \rightarrow -\infty$. Considering both series, F_a and F_b , as $v \rightarrow -1$, which occurs as $z \rightarrow -\infty$, we find that they have the same type of singularity, diverging at least as $\ln(1+v)$ but no worse than $(1+v)^{-1}$. To eliminate the singularity in order to render F finite as $v \rightarrow -1$, we first define

$$g_n = -b_n/a_n \tag{4.3}$$

and then choose

$$g = \lim_{n \rightarrow \infty} g_n. \tag{4.4}$$

In practice, g has to be computed to high accuracy since, as $v \rightarrow -1$, F_v is obtained from the difference between two extremely large numbers. In Appendix A, we show that this can be achieved efficiently using the following formula

TABLE III. Solutions required (or convenient to use) for different v_s .

Value of v at surface	$v_s \leq -2$	$-2 < v_s < 0$	$-1 < v_s < 1$	$v_s \geq 1$
Solution	u, y	y	v	u, v , and y
Matching points	$-2 < v_m < -1$			$-1 < v_{m1} < 0$ $0 < v_{m2} < 1$

$$g = g_N + \frac{1}{2}(q + \alpha^2) \left[(2\alpha - 1) \sum_{n=N+1}^{\infty} n^{-2} - (1 - 6\alpha + 4\alpha^2 - 2q) \sum_{n=N+1}^{\infty} n^{-3} \right] + O(N^{-3}). \quad (4.5)$$

The procedure is to compute first g_n iteratively using (4.3) to a reasonably large N (dictated by the accuracy needed), and then include the correction term given above. The remaining error is of the order of N^{-3} . With g known, the continuity of H_y at $z = 0$ results in

$$A_v = H_{ys}/F_v(v_s), \quad (4.6)$$

and the continuity of E_x yields a dispersion relation in the form of (4.1) with F_v replacing F . In the limit $v_s \rightarrow 0$, which occurs if $\epsilon_s \rightarrow 0$ or $\omega \rightarrow \omega_{ps}$, an approximate dispersion relation can be obtained by considering only the first few terms of the series. Furthermore, if $|q| \ll |\alpha| \ll 1$, which is not difficult to achieve experimentally, we find that $g \cong -\alpha$. The resulting approximate dispersion relation is very simple:

$$\beta/\epsilon_2 = -(\alpha/\epsilon_1)[1 + \alpha(1 + v_s - \ln v_s)]. \quad (4.7)$$

For real dielectric constants, the $\ln v_s$ term in the above expression is replaced by $\ln|v_s|$. This singular term will be found to have a profound effect on the dispersion relation, particularly in the case of depletion layers. We shall return to this later.

B. Use of y solution for $-2 < v_s < 0$

Referring to Table I, we find the y solution can be used alone for all $z < 0$ if $-2 < v_s < 0$, with the applicable frequency ranges given in Table II. The continuity of H_y at $z = 0$ yields

$$A_y = H_{ys}/F_y(v_s) \quad (4.8)$$

and the continuity of E_x results in a dispersion relation also in the form of (4.1) with F_y replacing F .

$$\begin{pmatrix} F_y(v_{m1}) & -F_b(v_{m1}) & -F_a(v_{m1}) & 0 \\ F'_y(v_{m1}) & -F'_b(v_{m1}) & -F'_a(v_{m1}) & 0 \\ 0 & F_b(v_{m2}) & F_a(v_{m2}) & -F_e(v_{m2}) \\ 0 & F'_b(v_{m2}) & F'_a(v_{m2}) & -F'_e(v_{m2}) \end{pmatrix} \begin{pmatrix} A_y/A_u \\ A_v/A_u \\ gA_v/A_u \\ h \end{pmatrix} = \begin{pmatrix} 0 \\ 0 \\ F'_d(v_{m2}) \\ F'_d(v_{m2}) \end{pmatrix}, \quad (4.12)$$

with A_u given again by (4.9). The dispersion relation is still in the form (4.1) with F_u replacing F .

As noted above, the use of either one or more solutions in different ranges of v_s , which is summarized in Table III, is not unique but may be more convenient. When more than two solutions are

This dispersion relation has been studied extensively.⁶⁻⁹

C. Matching u and y solutions for $v_s \leq -2$

According to Table I, the u solution alone should be valid for all $z < 0$ if $v_s \leq -2$. This is true provided the integration constant h can be properly determined, the problem being similar to that of determining g in the v solution. However, for some obscure reason, we failed to obtain reasonable results using the u solution alone. Fortunately, the difficulty can be entirely avoided if we choose a matching value v_m , satisfying $-2 < v_m < -1$, to join the u and y solutions so that the continuity of the tangential electric and magnetic fields is maintained there. Thus the u solution was used near the surface (in $v_s \leq v \leq v_m$) and the y solution deep in the bulk (in $v_m \leq v < -1$). The unknown integration constants are found to be

$$A_u = H_{ys}/F_u(v_s), \quad (4.9)$$

$$A_y = A_u[(F_d F'_e - F'_d F_e)/(F_y F'_e - F'_y F_e)]_{v=v_m}, \quad (4.10)$$

$$h = -[(F_y F'_d - F'_y F_d)/(F_y F'_e - F'_y F_e)]_{v=v_m}. \quad (4.11)$$

The dispersion relation is again in the form (4.1) with F_u replacing F .

D. Matching u, v , and y solutions for $v_s \geq 1$

If $v_s \geq 1$, we may choose to use only u and v solutions and match at a point between 0 and 1. But we have found that much faster computation can be achieved if all three solutions are used. The entire range of $-1 < v < v_s$ is divided into three pieces by two matching points v_{m1} and v_{m2} which satisfy $-1 < v_{m1} < 0 < v_{m2} < 1$. The y solution can then be used deep in the bulk (in $-1 < v \leq v_{m1}$), the u solution near the surface (in $v_{m2} \leq v \leq v_s$), and the v solution in the middle (in $v_{m1} \leq v \leq v_{m2}$). Applying the boundary conditions, we find that the five integration constants satisfy the following matrix equation:

joined, we are free to choose the exact location of the matching points. Such freedom turns out to be extremely valuable for double checking the numerical results. As an important example, it is worth noting that in the case of $|v_s| < 1$, although the v solution can be used alone as treated in Sec. IVA, we

can do as well by matching y and v solutions together at an arbitrary matching point between -1 and 0 . In fact since g needs to be computed to very high accuracy, as noted earlier, it is very often faster to obtain it through matching y and v solutions rather than using Eq. (4.5) and iteration.

V. DEPLETION LAYERS

Since $\epsilon_I \ll \epsilon_R$, except for a small region close to where ϵ_R vanishes, we first evaluate the dispersion for real ϵ . Even this requires lengthy computer calculations, as indicated in Sec. IV. In this section we present some typical results for depletion layers at the surface, first for real ϵ , then for complex ϵ . A few of the results of this section have been reported in preliminary form.¹⁶

A. Dispersion for real ϵ

For a depletion layer the surface value of plasma frequency $\omega_{ps} < \omega_{pb}$. Note, however, that ω_{ps} cannot equal 0 as assumed by CMW.⁵ Just what ω_{ps} is depends on the location of the band edges relative to the Fermi level at the surface, which is affected by surface states, external fields, exposure to ambients, surface treatments, etc. Consider an InSb sample similar to those investigated in Ref. 1, with bulk carrier concentration N_b in the range $(1-7) \times 10^{18}/\text{cm}^3$. With an average m^* for electrons of $0.03 m_0$, m_0 being the free-electron mass, and $\epsilon_\infty = 16$, this leads to ω_{pb} in the range $8 \times 10^{13} - 2 \times 10^{14} \text{ sec}^{-1}$. At room temperature in InSb the thermal-equilibrium product of electron concentration N and hole concentration P is $\sim 5 \times 10^{32}/\text{cm}^6$.¹⁷ The hole concentration in the bulk is then $\sim 10^{-5} N_b$ for the sample we are considering. Since the average hole mass is $0.16 m_0$, larger than the electron mass, the hole contribution to ω_{pb} is negligible. If the bands were flat to the surface, ω_{ps} would equal ω_{pb} . Usually, however, the bands curve upward in going from the interior to the surface, so that N and P at the surface are smaller and larger, respectively, than their bulk values. At 77°K in an InSb sample with undisturbed surface the curvature of the bands is considerable, the Fermi level at the surface lying at an energy $\frac{2}{3} E_g$ below the edge of the conduction band.¹⁸ If the Fermi level were similarly located at room temperature, the hole concentration at the surface would be ~ 5000 times the electron concentration there, and the hole contribution to ω_{ps} would be much more important than to ω_{pb} . With $E_g \approx 0.18 \text{ eV}$ at room temperature, we estimate the hole contribution to ω_{ps} to be $\sim 2-4 \times 10^{13} \text{ sec}^{-1}$, with the electron contribution perhaps $\frac{1}{10}$ as large. Thus ω_{ps}/ω_{pb} could range from about $\frac{1}{2}$ to $\frac{1}{10}$ for samples with N_b between $1 \times 10^{18}/\text{cm}^3$ and $7 \times 10^{18}/\text{cm}^3$, not far from

the flat-band value of unity. There is, however, another consequence of a large hole contribution to ω_{ps} : The total plasma frequency, which is the sum of electron and hole contributions, may no longer be represented accurately as a constant plus a single exponential decreasing monotonically from bulk to surface. Equation (1.1), on which our calculations are based, would then not describe the situation well very close to the surface. Of course, we do not have information about the location of the Fermi level at the surface at 300°K in any particular InSb sample, even one with an undisturbed surface. Knowing the energy gap and the electron and hole masses, we can, however, determine that the minimum value of ω_{ps} for InSb with a depletion layer is approximately $\frac{1}{10} \omega_{pb}$ at this temperature. Thus we expect $\omega_{pb} \geq \omega_{ps} \geq 0.1 \omega_{pb}$ for depletion layer samples.

Without knowledge of the curvature of the bands at the surface it is not possible to calculate d . At 77°K , for an undisturbed sample with $N_b \approx 1 \times 10^{18}/\text{cm}^3$, the information on the location of the Fermi level given above leads to $d \approx 250 \text{ \AA}$.¹⁹ For larger N_b , d would be smaller, decreasing approximately as $\sqrt{N_b}$. At room temperature the energy gap is considerably smaller and, for the same location of the Fermi level relative to the conduction band edge, d would be considerably smaller. We estimate it as no more than 100 \AA for N_b in the range $(1-7) \times 10^{18}/\text{cm}^3$. If the bands were less curved, d would be even less. For disturbed samples d would, of course, depend on the nature and the extent of the disturbance. In one study of an InSb sample with a grating cut on its surface, the authors obtained evidence, through etching, for a surface layer depth of 0.1 mm .²

We conclude that for InSb samples with $N_b = (1-7) \times 10^{18}/\text{cm}^3$ and undisturbed surfaces, ω_{ps}/ω_{pb} at room temperature is probably in the range $\frac{1}{10} - \frac{1}{2}$ and d is likely to be no more than 100 \AA . For disturbed samples d could be much larger. Values of ω_{ps}/ω_{pb} between the minimum and unity should be realizable by introduction of suitable electric fields or ambients. Much smaller ratios of ω_{ps} to ω_{pb} should be obtainable—in fact, usual—in materials with larger values of E_g , such as GaAs, since the thermal equilibrium NP product is proportional to $\exp(-E_g/kT)$.¹⁷ The smaller NP product will also result in Eq. (1.1) being a better approximation when the Fermi level at the surface is below midgap. In addition, d would be larger for larger bandgap materials.

As can be deduced from the dispersion relation (4.1), for given ϵ_2 and ϵ_∞ the dispersion depends only on the dimensionless quantities ω/ω_{pb} , ck_x/ω_{pb} , ω_{ps}/ω_{pb} , and $\omega_{pb} d/c$. Our results will therefore be given in terms of these quantities. In Fig.

1 we show the calculated dispersion for $\tau = \infty$, i.e., ϵ real, $\omega_{pd}d/c = 0.1$, and three different values of ω_{ps}/ω_{pb} . The value $\omega_{pd}d/c = 0.1$ corresponds to $d = 1500 \text{ \AA}$ for $\omega_{pb} = 2 \times 10^{14}/\text{sec}$, thus many times as large a value of d as expected for undisturbed InSb samples. This large value of d has been chosen because it allows the structure to be exhibited more clearly and, as discussed above, it is not unreasonable for disturbed samples, which may have still much larger d .

As can be partly seen with the help of the inset in Fig. 1, for $\omega_{ps}/\omega_{pb} = 0.6$ there is one branch that follows the light closely up to $\omega = \omega_{ps}$ and then approaches very closely the horizontal line $\omega/\omega_{pb} = 0.6$, although always staying below it. For this branch $\epsilon < 0$ everywhere, although it is very close to 0 at the surface. This is the usual surface-plasmon branch, or branch I in the nomenclature of Rice *et al.*¹⁶ Because the behavior near ω_{ps} is completely dominated by ϵ being very close to 0 at the surface, it was particularly reassuring to find that the y solution gave the same results as the v solution for this case. In the limit of large k_x (beyond what is shown in Fig. 1) branch I curves down and goes asymptotically to the frequency ω ,

at which $\epsilon_s = -1$, i.e., $\omega_{ps}[\epsilon_\infty/(\epsilon_\infty + 1)]^{1/2}$. This is readily deduced as follows, from the use of (4.1) with the y solution. In the limit $k_x \rightarrow \infty$, $(F'_y/F_y)_{z=0}$ approaches a constant value, but $\alpha \rightarrow \infty$, so the expression in angular brackets in (4.1) approaches unity. The resulting dispersion relation can only be satisfied by $\epsilon_s \rightarrow -\epsilon_2$,⁹ which is -1 in this case. The branch labeled II(0.6) lies everywhere above $\omega = 0.6\omega_{pb}$, thus corresponds to ϵ being positive at the surface, having gone through 0 just below it. Where branches I and II are close to each other, $|v_s|$ is very close to 0. The existence for small $|v_s|$ of a closely spaced pair of branches, almost symmetric with respect to $v_s = 0$, or $\omega = \omega_{ps}$, is the result of the $\ln v_s$ term in Eq. (4.7). For the case of real ϵ , now being considered, $\ln v_s$ becomes $\ln |v_s|$, which is so large for $|v_s|$ close to 0 that it dominates the right-hand side of (4.7) and thus the behavior of the dispersion. It should also be noted that for real ϵ no dispersion curve can cross the line $\omega = \omega_{ps}$. This is the case because the \ln term is infinite at $v_s = 0$, which corresponds to E_x being infinite at $z = 0$, making it impossible to satisfy the dispersion relation.

We also find a third branch, labeled III(0.6), which joins II(0.6) near $ck_x/\omega_{pb} = 0.62$. The same type of structure, with a pair of branches just above and below $\omega = \omega_{ps}$ and a higher third branch, is always found for ω_{ps} values less than $0.6\omega_{pb}$. In the limit $\omega_{ps} \rightarrow 0$ branch III corresponds to the dispersion curves calculated by CMW, although theirs differ in detail since they approximate ϵ by a piecewise linear function.

For $\omega_{ps} = 0.92\omega_{pb}$ the dispersion consists of branch I for $\omega < \omega_{ps}$ plus a closed loop for $\omega_{ps} < \omega < \omega_{pb}$. We may still define branches II and III by taking as the boundaries between them the two endpoints where the loop is tangent to a vertical line. The case $\omega_{ps} = 0.8\omega_{pb}$, shown in Ref. 16, has a branch II-III structure intermediate between those of 0.6 and $0.92\omega_{pb}$. For $\omega_{pd}d/c$ ten times as large, the case shown in Fig. 2, we see the same types of structures with the branch III's in general closer to the branch II's. The structure formed by branches II(0.6) and III(0.6) now also appears to be a closed loop, with the joining at somewhat larger k_x than shown. From the experience of seeing many such structures, plus the results of an integral equation approach,²⁰ we believe that the closed-loop behavior for branches II and III is quite general, although the joining may come at very large k_x . In general, the loop shrinks gradually with increasing ω_{ps}/ω_{pb} . It disappears for some frequency ω_{ps} close to ω_{pb} , and for frequencies beyond this only branch I appears. For the parameters of Fig. 2 the value of ω_{ps} for which it disappears is in the range $0.9\omega_{pb} > \omega_{ps} > 0.8\omega_{pb}$, while for those of Fig. 1 it disap-

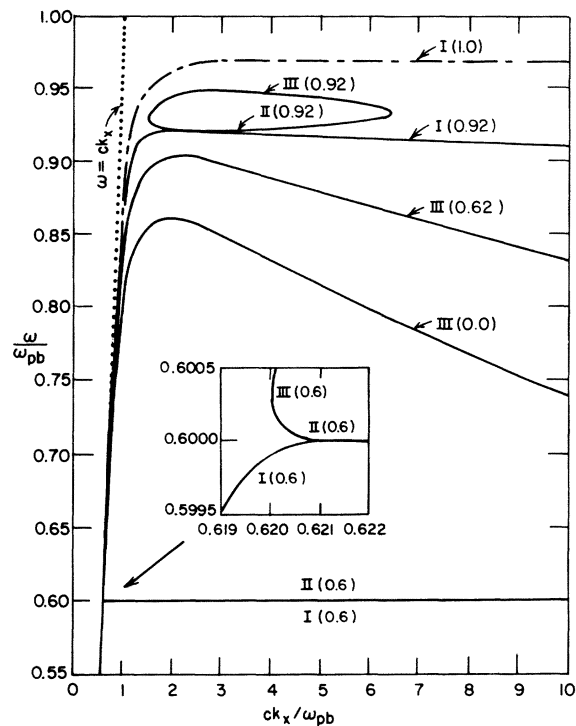


FIG. 1. Dispersion in normalized units for the case of a depletion layer on a sample with $\omega_{pd}d/c = 0.1$, $\epsilon_\infty = 16$, $\epsilon_2 = 1$, $\tau = \infty$, and $\omega_{ps}/\omega_{pb} = 0.6, 0.92, 1.0$. The latter is shown as a dash-dotted curve. The result for $\omega_{ps}/\omega_{pb} = 0$ is shown for reference. The inset is an expanded view of the neighborhood of $\omega = \omega_{ps}$ for $\omega_{ps}/\omega_{pb} = 0.6$.

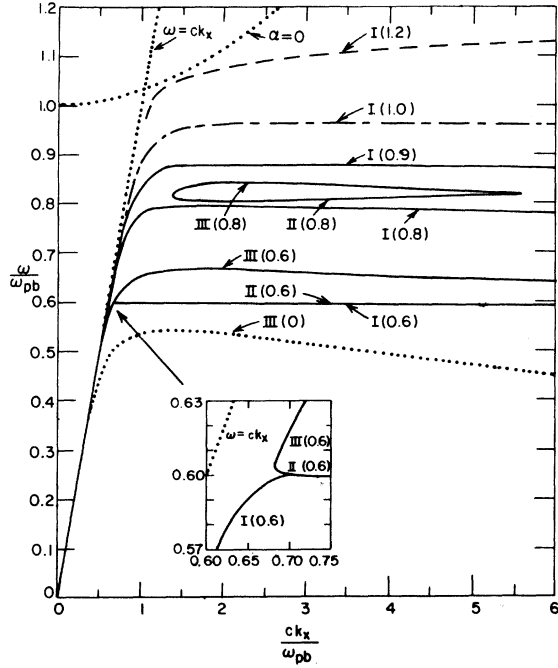


FIG. 2. Dispersion in normalized units for the case of a depletion layer on a sample with $\omega_{pb}d/c=1$, $\epsilon_\infty=16$, $\epsilon_2=1$, $\tau=\infty$, and $\omega_{ps}/\omega_{pb}=0, 0.6, 0.8, 0.9, 1.0$. The lower inset is an expanded view of the neighborhood of $\omega = \omega_{ps}$ for $\omega_{ps}/\omega_{pb} = 0.6$. Shown for contrast is the case $\omega_{ps}/\omega_{pb} = 1.2$, which corresponds to an accumulation layer.

pears in the range $\omega_{pb} > \omega_{ps} > 0.92\omega_{pb}$.

The dispersion for parameters that come closer to representing the InSb samples we were discussing earlier, with undisturbed surfaces, is shown in Fig. 3. $\omega_{pb}d/c=0.02$ corresponds to $\omega_{pb}=2 \times 10^{14}/\text{sec}$ ($N_b=7 \times 10^{18}/\text{cm}^3$) and $d=300 \text{ \AA}$, while $\omega_{pb}d/c=0.043$ corresponds to 650 \AA for the same ω_{pb} . Because of the small values of $\omega_{pb}d/c$, the branch III's are now quite close to the $\omega_{ps}=\omega_{pb}$ line. In fact, the difference between branch III for $\omega_{ps} \leq 0.3\omega_{pb}$ and for $\omega_{ps}=0$ is not discernible on the scale used for the figure. The loop formed by branches II and III for $\omega_{ps}=0.1\omega_{pb}$ is a very large one.

We summarize briefly the behavior for samples with depletion layers seen for real ϵ . With increasing $\omega_{pb}d/c$ the approximately horizontal portion of branch III calculated for $\omega_{ps}=0$ moves further below that for the homogeneous sample ($\omega_{ps}=\omega_{pb}$). All the structure for depletion layers with $\omega_{ps} \neq 0$ —the branch I's reaching their highest points in a plateau just below $\omega = \omega_{ps}$ and the loops lying above $\omega = \omega_{ps}$ —lies between III(0) and the homogeneous sample line. The loops are very large for $\omega_{ps} \ll \omega_{pb}$ and decrease in size with increasing ω_{ps}/ω_{pb} until they disappear for some ω_{ps} close to ω_{pb} .

B. Electric and magnetic field behavior

The significance of branches I, II, and III becomes clearer when we consider the variation with z of the fields associated with each branch. In the frequency range of branches II and III, ϵ_R vanishes somewhere in the sample. If, still neglecting ϵ_I for the time being, we use the v solution to describe the field behavior in the neighborhood of z_0 , the value of z for which ϵ_R vanishes, we obtain

$$H_y = A_v \left(\frac{v+1}{v_s+1} \right)^\alpha \left\{ 1 - \alpha v + \left[g - \frac{1}{4}(q - 4\alpha + \alpha^2) + \frac{1}{2}(q + \alpha^2) \ln|v| \right] v^2 + \dots \right\}, \quad (5.1)$$

$$E_x = A_v \left(\frac{i}{2\omega d \epsilon_b} \right) \left(\frac{v+1}{v_s+1} \right)^\alpha \left[4g + q + 2\alpha - \alpha^2 + 2(q + \alpha^2) \ln|v| + \dots \right], \quad (5.2)$$

$$E_z = (k_x/\omega \epsilon_b v) H_y. \quad (5.3)$$

Here we have used the relation $\exp(p_\sigma z) = [(v+1)/(v_s+1)]^\alpha$. Differentiating H_y in (5.1) with respect to v , we find that the magnetic field has an ex-

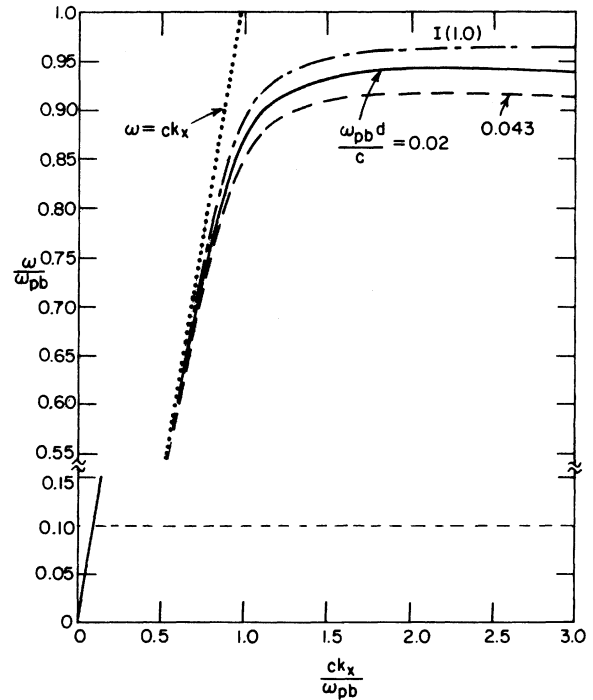


FIG. 3. Dispersion in normalized units for depletion-layer cases with $\omega_{ps}/\omega_{pb} = 0.1$, $\omega_{pb}d/c = 0.02, 0.043$, $\epsilon_\infty = 16$, $\epsilon_2=1$, $\tau=\infty$. The dot-dashed line represents $\omega_{ps}/\omega_{pb} = 1$.

tremum at $z = z_0$. At the same place E_x , according to (5.2) shows a logarithmic singularity and E_z diverges as v^{-1} . The singularities are, however, due to use of real ϵ and will be seen to disappear when we introduce damping.

To demonstrate the behavior of the fields, we show in Fig. 4 H_y and E_x vs z for the three branches at the same value of k_x . In all cases, for large enough z we expect, according to (3.3), decay as $\exp(-\rho_0 z)$. For branch I, essentially the usual plasmon branch, H_y and E_x both decay monotonically, more or less as exponentials, below the surface. For branches II and III both H_y and E_x rise initially below the surface and, as predicted, H_y has a maximum and $E_x \rightarrow \infty$ at $z = z_0$ before decaying exponentially. The difference between II and III is that $\epsilon = 0$ is closer to the surface in the former case, corresponding to smaller $|v_s|$.

C. Effect of damping

As discussed earlier, for $\omega\tau \gg 1$, ϵ_I , defined in Eq. (2.1), is small compared to ϵ_R except in the neighborhood where ϵ_R vanishes. Thus the effects of damping will be significant only for ω close to ω_{ps} or $|v| \ll 1$. In that neighborhood the dispersion is given by (4.7). In obtaining the results discussed so far in this section we have considered $\ln v_s$ to be

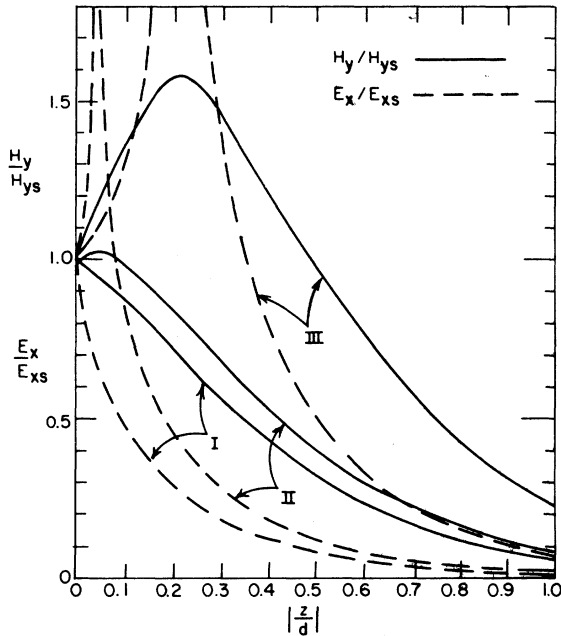


FIG. 4. Electric and magnetic field amplitudes, normalized to the surface values, versus normalized depth below the surface for the case $\omega_{pb}d/c=1$, $\epsilon_\infty=16$, $\epsilon_2=1$, $\tau=\infty$, $\omega_{ps}/\omega_{pb}=0.8$. The fields are shown for $ck_x/\omega_{pb}=3$, which corresponds to $\omega/\omega_{pb}=0.79371$ for branch I, 0.80912 for branch II, 0.84215 for branch III.

replaced by $\ln|v_s|$. The effect of complex ϵ on the terms in (4.7) will be by far the largest on the \ln term, so we will neglect the effect on the other terms. The real part of $\ln v_s$ becomes $\frac{1}{2} \ln(v_{sR}^2 + v_{sI}^2)$, the subscripts R and I denoting real and imaginary parts. Damping will have significant effect where $|v_{sI}| \gtrsim |v_{sR}|$. For $\omega\tau \gg 1$ and $\omega \approx \omega_{ps}$ we find from Eq. (2.1)

$$(v_{sI}/v_{sR}) \approx [2\tau(\omega_{ps} - \omega)]^{-1}. \quad (5.4)$$

In regions where ω is so close to ω_{ps} that $|v_{sI}/v_{sR}| \gtrsim 1$ it is likely that the dispersion relation (4.7) will no longer be satisfied for complex ϵ because the \ln term is prevented from approaching ∞ . When $|v_{sI}/v_{sR}| < 1$ the dispersion should be little affected. We should, therefore, get a good approximation to the effect of damping by eliminating those portions of the dispersion curves for which $|v_{sI}/v_{sR}| \geq 1$. This wipes out the portions of branches I and II that were very close together, resulting in the three branches forming a single reentrant curve. Figure 5 shows the dispersion of Fig. 1 after the introduction of what seems physically reasonable damping, corresponding to $\tau = 5 \times 10^{-13}$ /sec, for $\omega_{pb} = 10^{14}$ /sec, or $\tau = 10^{-13}$ /sec for $\omega_{pb} = 5 \times 10^{14}$ /sec, etc. In the k_x region where I and II were very close together the dispersion is represented by branch III. At large k_x , for $\omega < \omega_{ps}$, branch III goes over into what is left of branch I. The asymptotic behavior in the limit of large k_x is that of branch I, i.e., the dispersion approaches the limiting frequency $\omega_{ps}[\epsilon_\infty/(\epsilon_\infty + \epsilon_2)]^{1/2}$. The reentrant feature for ω_{ps} close to ω_{pb} and the approach to the asymptotic behavior should be experimentally detectable.

As noted earlier, damping also wipes out the singularities in the electric fields. For E_x/E_{xs} , to a good approximation [see Eq. (5.2)], the actual peak height will be reduced from ∞ to $\ln|v_I(z_0)|/\ln|v_{sR}|$, since v_s at the surface is not far from 0 for the cases being discussed. From the definitions of v and $\epsilon(z)$ we deduce that $\ln|v_I(z_0)| = \ln|v_{sI}/(v_{sR} + 1)|$. The quantities v_{sI} and v_{sR} may be calculated from ω , ω_{ps} , ω_{pb} , and $1/\omega\tau$. For $\omega_{pb}\tau = 50$ in the two cases of Fig. 4 we obtain $v_{sI}/(v_{sR} + 1) \approx 0.05$. With $v_s = 0.425$ for II, 0.238 for III, we conclude that the peak in curve II is just about fully suppressed, while that in III is not. For curve III $E_x(z_0)/E_{xs} \approx 2$. Neither the location of the peak nor the fields away from $z = z_0$ are much affected by the small damping characteristic of large $\omega\tau$.

D. Comparison with experiment

The parameters in Fig. 3, as noted earlier, were chosen to more or less resemble those of the samples in the surface-plasmon dispersion

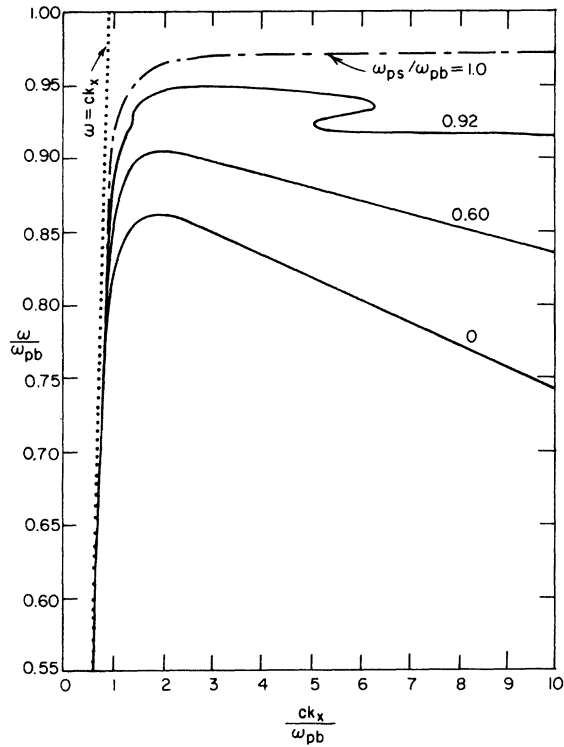


FIG. 5. Dispersion in normalized units for the depletion-layer case of Fig. 1 with finite τ (damping) corresponding to $\omega_p \tau = 50$ ($\tau = 5 \times 10^{-13}$ sec for $\omega_p = 10^{14}$ /sec). The number associated with each curve is ω_{ps}/ω_{pb} for that case.

studies of Ref. 1 and 3. Of course, ω_{ps} is not known but, as discussed earlier, on the assumption of an undisturbed surface ω_{ps}/ω_{pb} in the range $\frac{1}{10}$ – $\frac{1}{2}$ is not unreasonable. If we correct for ϵ being complex, with a reasonable τ for the InSb samples concerned, the horizontal dashed lines at ω_{ps} , representing branches I and II, disappear. The dispersion for $\omega_{pb}d/c = 0.02$ is then given by the solid line, actually branch III, for the k_x range shown. The dispersion in this range of k_x is not particularly sensitive to ω_{ps} for, as noted earlier, it would not be possible to distinguish, on the scale used, between branch III for any $\omega_{ps} \leq 0.3\omega_{pb}$ and branch III for $\omega_{ps} = 0$. In the experimental study of Ref. 1, Marshall *et al.* used an inscribed line grating on their samples, with grating spacings in the range 10–30 μm , to introduce the SPP's. Their results were compared with the predicted dispersion for a sample homogeneous to the interface. The data were found to follow the light line well at low frequencies, but in the region where the dispersion curve falls below the light line and in the plateau region, the points lay below the homogeneous sample dispersion by several percent. In the later experiments,³ a prism was used to introduce the

SPP's, leaving the InSb surface undisturbed. In this case the experimental points in the plateau region are found to lie within about $\frac{1}{2}\%$ of the homogeneous sample dispersion, still below it. Fischer *et al.*³ attributed their earlier data to a depletion layer created by mechanical destruction of the surface required to create the grating. They state that, for the earlier data, "it is, in fact, possible to fit the experimental points by a dispersion curve which is calculated for a surface having a depletion layer of about 1 μm in depth," with average carrier concentration in this layer assumed at least an order-of-magnitude lower than the bulk. They comment, reasonably, that "The value of 1 μm , as deduced from a simple step model for the depletion, however, appears surprisingly large for such heavily doped semiconductors."

To compare these experimental results with those in Fig. 3, we note first that, for the small values of d in the figure and fixed ω_{ps} , the amount by which the more-or-less horizontal region of the curves for finite d lies below the curve for the homogeneous sample ($d = 0$) varies linearly with d . As mentioned earlier, for $\omega_{pb} = 2 \times 10^{14}$ /sec ($N_b \approx 7 \times 10^{18}$ /cm³), $\omega_{pb}d/c = 0.02$ corresponds to $d = 300$ Å, while $\omega_{pb}d/c = 0.043$ corresponds to 650 Å. Consistent with the statement just made above, for ck_x/ω_{pb} between about 1.5 and 3, $\omega_{pb}d/c = 0.02$ lies $\sim 2\frac{1}{2}\%$ below the homogeneous sample curve while $\omega_{pb}d/c = 0.043$ lies a little over 5% below. To achieve a dispersion curve lying within $\sim \frac{1}{2}\%$ below the homogeneous sample curve for $\omega_{ps}/\omega_{pb} \leq 0.3$ would require $d \leq 60$ Å. If ω_{ps}/ω_{pb} were larger, d could be somewhat larger. The fact that Eq. (1.1) might not hold very close to the surface for this case because of inversion, i.e., $P > N$ at the surface, should matter little since d is so small. Thus the experimental data for the case of prism introduction³ correspond more or less to our expectations for a sample with undisturbed surface at 300 °K. For the case of the samples with the gratings we deduce from Fig. 3 $d \sim 350$ – 400 Å for $\omega_{ps}/\omega_{pb} = 0.1$. This is clearly a more reasonable result than the 1- μm depth from the step model.

Clearly, comparison of SPP dispersion with theory provides a technique for learning about the depth of disturbance in samples with disturbed surfaces, even when these depths are relatively small. In addition, despite the small d values, it should still be possible to get some information on ω_{ps} if the experimental data were taken to larger k_x . For one thing it might be possible to observe the reentrant feature predicted at $\omega = \omega_{ps}$. Even if this is not possible, it should be possible to get information, even for undisturbed surfaces, from the approach to the asymptotic frequency ω ,

$= \omega_{ps} [\epsilon_\infty / (\epsilon_\infty + \epsilon_2)]^{1/2}$. Data could easily be taken to much larger values of k_x than attained in Ref. 1 and 3 by means of recently developed holographic techniques for making gratings with much smaller spacings. Such gratings can be made with spacings less than $\frac{1}{2}$ the wavelength of the argon blue laser, thus 50 times smaller than the finest used in Ref. 1.²¹

E. Guided modes

For samples with $\omega_{pb}d/c \geq \frac{1}{3}$ (with $\epsilon_\infty = 16$, $\epsilon_2 = 1$, $\omega_{ps} = 0$) we found additional branches in the dispersion corresponding to guided modes, i.e., modes in which the field amplitudes are oscillatory below the surface before decaying exponentially as $z \rightarrow -\infty$.¹⁰ These branches always start at the light line, $k_x = \sqrt{\epsilon_2}\omega/c$, sometimes for $\omega < \omega_{pb}$. They are discussed in another publication.¹²

VI. ACCUMULATION LAYERS

In the case of an accumulation layer ($\omega_{ps} > \omega_{pb}$) there can be no guided plasmon modes, but a second surface-plasmon branch has been found. One branch of the dispersion due to an accumulation layer, with $\omega_{ps}/\omega_{pb} = 1.2$, has already been shown in Fig. 2. We label this branch I because it looks like a natural continuation of the depletion-layer series with increasing ω_{ps} . However, unlike branch 1 for depletion layers, it may, and in this case actually does, rise into the frequency range where ϵ is positive in part of the sample. This branch was also described by Rice *et al.*⁶ and by CMW. Note, however, that although both these sources plotted results for cases where the dispersion curve attained frequencies greater than ω_{pb} , so that ϵ goes through 0 inside the sample, they used only solutions valid for $\epsilon < 0$ everywhere. They nevertheless got reasonable-looking dispersion for this branch because they happened to choose cases where $\epsilon = 0$ is far enough away from the surface so that the solutions at $z = 0$, which determine the dispersion, were not much affected.

As seen in Fig. 2, branch I for $\omega_{ps} = 1.2\omega_{pb}$ starts from the light line at low frequencies, rises above the limiting frequency for the homogeneous sample, and above ω_{pb} , until it comes close to the corner where the line $\alpha = 0$ crosses the light line, and then flattens. The fact that the limiting frequency ω_l for an accumulation layer must lie above the homogeneous sample curve I(1.0) was pointed out by Rice *et al.*⁶ and by one of us⁸ for the case $|\Delta\epsilon/\epsilon_b| \ll 1$. By the same type of reasoning as was used in Sec. VA for depletion layers, we can show that, if the y solution is valid at the surface, in the limit $k_x \rightarrow \infty$ the limiting frequency $\omega_l = \omega_{ps} [\epsilon_\infty / (\epsilon_\infty + \epsilon_2)]^{1/2}$ is also attained for accumulation layers.

However, as can be deduced from Table II, for accumulation layers the y solution does not converge for $\omega_{ps} > \omega > \omega_{pb}$ nor even for ω somewhat less than ω_{pb} . We have been able to show, by means of an integral equation approach,²⁰ the above expression for ω_l is nevertheless valid in these frequency ranges also. Although we do not plot Fig. 2 to large enough values of k_x to demonstrate this for I(1.2), our calculations verify that it is heading for such a value of ω_l .

To see the second branch for the parameters of Fig. 2 requires an expanded scale in the neighborhood $\omega/\omega_{pb} = 1$. This is shown in Fig. 6 for three values of ω_{ps}/ω_{pb} , the other parameters being the same as those of Fig. 2. For $\omega_{ps}/\omega_{pb} = 1.1$ we find a second branch, labeled II(1.1) in the corner formed by $\alpha = 0$ and the light line. As ω_{ps}/ω_{pb} increases, branches I and II come closer together. At $\omega_{ps} = 1.3\omega_{pb}$ and beyond there is a sharp kink in both branches I and II, separating regions of different slopes. Similar behavior can be observed for varying $\omega_{pb}d/c$. In Fig. 7 we show the dispersion curves for several values of $\omega_{pb}d/c$ with ω_{ps}/ω_{pb} fixed at 1.2 and the other parameters the same as Fig. 6. At $\omega_{pb}d/c = 0.1$ a tiny branch II appears in the corner formed by the light line and $\alpha = 0$. With increasing $\omega_{pb}d/c$ we find branches I and II moving closer. For $\omega_{pb}d/c \geq 1.5$, the two branches show the sharp kinks seen in Fig. 6 for $\omega_{ps} = 1.3\omega_{pb}$.

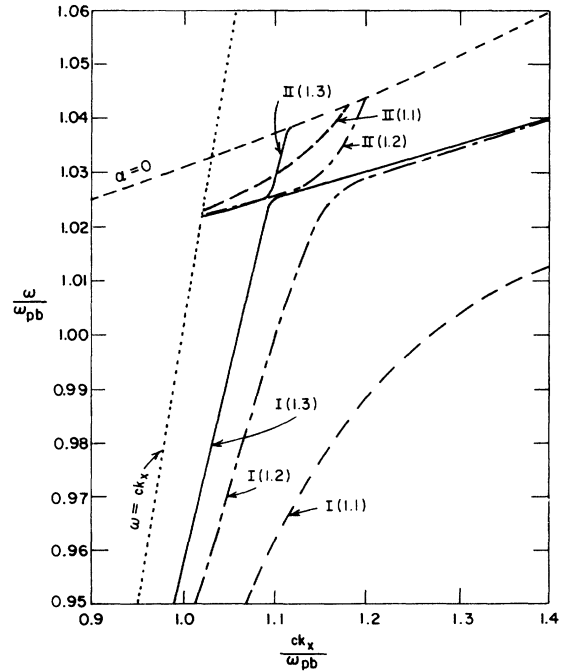


FIG. 6. Dispersion in normalized units for an accumulation-layer case with $\omega_{pb}d/c = 1$, $\epsilon_\infty = 16$, $\epsilon_2 = 1$, $\tau = \infty$, and ω_{ps}/ω_{pb} values of 1.1, 1.2, 1.3.

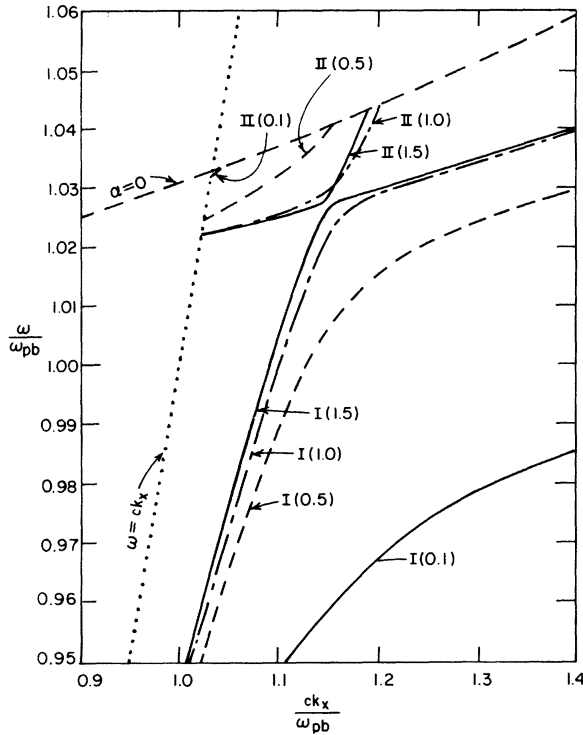


FIG. 7. Dispersion in normalized units for an accumulation-layer case with $\epsilon_\infty = 16$, $\epsilon_2 = 1$, $\tau = \infty$, $\omega_{ps}/\omega_{pb} = 1.2$ and $\omega_{pb} d/c$ values of 0.1, 0.5, 1.0, and 1.5.

Note that ω vs k_x for branch II curves upward, in the opposite direction from that claimed by Rice *et al.* for an accumulation layer.⁶

The small range of frequencies in which branch II appears in these figures is due to the large value of ϵ_∞ . Branch II must be contained between ω_{pb} on one side and $\alpha = 0$ on the other. The $\alpha = 0$ line crosses the light line at $\omega = \omega_{pb}[\epsilon_\infty/(\epsilon_\infty - 1)]^{1/2}$. For large ϵ_∞ the crossing frequency is only slightly larger than ω_{pb} . In a material with smaller ϵ_∞ there would be more of a frequency range for branch II, which should make it easier to observe.

It is also noteworthy that there is no special feature or structure, for either of the accumulation-layer branches, associated with $\omega = \omega_{pb}$ or ω_{ps} . Presumably the reason for this in the former case is that, when ω crosses ω_{pb} , the zero in ϵ_R enters the sample at large negative z , far from the surface, and thus does not particularly affect the fields at $z = 0$ and the dispersion. No effect can be expected at $\omega = \omega_{ps}$, where the zero reaches the top surface, since the dispersion curve does not reach such high frequencies, the limiting ω being determined by the condition $\epsilon_s = -1$. As a corollary, the dispersion shown for the accumulation-layer case, calculated for real ϵ , will be essential-

ly unaffected by moderate damping.

It is not difficult to understand the origin of the second branch. From (3.1), (3.5), (2.4), and the requirements of continuity of H_y and E_x at $z = 0$, we deduce that

$$\left(\frac{dH_y/dz}{H_y}\right)_{z=0} = -\frac{\epsilon_s}{\epsilon_2} p_2. \quad (6.1)$$

Thus, for a depletion layer, when $\epsilon_s > 0$, H_y initially increases below the surface ($z < 0$), as seen in Fig. 4. For an accumulation layer, when $\epsilon_s < 0$, H_y initially decreases. The latter behavior can be seen in Fig. 8 for several different sets of parameters. For $\omega = 0.9\omega_{pb}$ we see below the surface a monotonic decrease of $H_y(z)$, ultimately as $\exp(p_0 z)$. When $\omega_{ps} > \omega > \omega_{pb}$, $\epsilon_s < 0$, and $\epsilon_b > 0$ and there is the additional requirement that H_y go through an extremum at $\epsilon_R = 0$, or $z = z_0$. This, combined with the requirements on the initial slope and of ultimate exponential decay, leaves two possibilities for the magnetic field behavior: (i) H_y decreases below $z = 0$ until it goes through 0, reaches a minimum and then decays as $\exp(p_0 z)$; (ii) H_y starts decreasing below $z = 0$ but with increasing depth decreases less rapidly until its slope changes sign and it increases. It then goes to a maximum at z_0

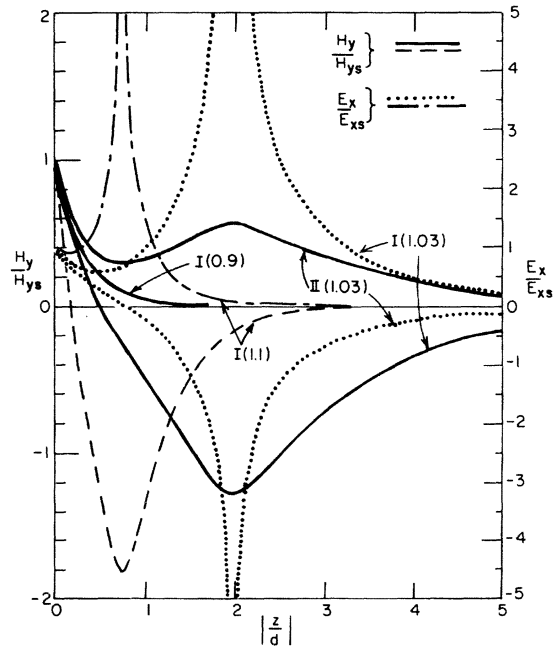


FIG. 8. Electric and magnetic field amplitudes, normalized to the surface values, versus normalized depth below the surface for the cases $\omega_{pb}d/c = 1$, $\epsilon_\infty = 16$, $\epsilon_2 = 1$, $\tau = \infty$, $\omega_{ps}/\omega_{pb} = 1.2$ and $\omega/\omega_{pb} = 0.9, 1.03, 1.1$, as indicated. The values of ck_x/ω_{pb} are 0.94373 for I(0.9), 1.21603 for I(1.03), 2.79301 for I(1.1), and 1.15231 for II(1.03).

and subsequently decays as $\exp(p_0 z)$. These two possibilities coincide with branches I and II, respectively, as shown in Fig. 8 for a case with $\omega = 1.03\omega_{pb}$. The extrema come at the same $|z/d|$ for these two branches because the parameters that determine z_0 [see Eq. (2.6)] are the same for the two. For $\omega = 1.1\omega_{pb}$ only branch I occurs, and the field variation is compressed in $|z/d|$ since $\epsilon_R = 0$ is closer to the surface. Corresponding to the extrema in H_y , there are singularities in E_x , which of course are removed by the existence of damping. These singularities differ from those seen in Fig. 4, the depletion-layer case, in that the singularity in E_x here is of the opposite sign to the extremum in H_y of the same branch. This occurs for branch II because where H_y goes through a minimum, dH_y/dz vanishes and therefore E_x goes from positive to negative. In the case of branch I, even though H_y becomes negative, its derivative vanishes only where $\epsilon = 0$, so E_x belonging to branch I must stay positive.

A striking feature of the dispersion in Figs. 6 and 7 is the presence of the sharp kink in both I and II for the highest values of ω_{ps}/ω_{pb} . With the help of Eq. (6.1) it can be seen that for these curves, as k_x moves toward the kink from smaller values, the magnitudes of the initial downward slopes of H_y for branches I and II move toward each other, becoming almost identical at the kink. Beyond the kink, with further increase in k_x the initial downward slopes move away from each other, that for I getting steeper, II less steep. For the curves without the kink $|\epsilon_s|$ is not large, the initial descent rates are not large and they continue to steepen with increasing k_x until branch II is cut off by reaching the $\alpha = 0$ line.

Samples to test the predictions of this section should be attainable, for example, by introducing donors into *n*-GaAs by diffusion or ion bombardment.

VII. CONCLUSIONS

We have extended the theory of SPP's on semiconductors to cover actual surfaces, having depletion or accumulation layers, with a physically reasonable model. For depletion layers we find, when moderate damping is included, that the dispersion corresponding to SPP's has a single branch. Like the case of the homogeneous sample, this branch starts by following the light line. For k_x not much larger than ω_{pb}/c it goes into an approximately horizontal region that lies below the plateau for the homogeneous sample case, the more so the larger the width of the depletion region and the smaller ω_{ps} . With increasing k_x , the dispersion curve drops further below the homogeneous sample plateau and

may display a reentrant region for $\omega \approx \omega_{ps}$. Asymptotically it goes to the limiting frequency $\omega_{ps}[\epsilon_\infty/(\epsilon_\infty + \epsilon_2)]^{1/2}$. For the frequencies at which $\epsilon < 0$ throughout the sample, i.e., $\omega < \omega_{ps}$, the magnetic field behaves much like that of the usual SPP, decaying essentially exponentially inside the material. Actually, for the depletion layer the initial decay is somewhat less rapid than exponential. For ω between ω_{ps} and ω_{pb} , the magnetic field peaks about where the real part of ϵ goes through 0. In this frequency range, therefore, we can consider that we have an SPP bound to the interface between positive and negative ϵ_R .

For large enough $\omega_{pb}d/c$ there may be, in addition to the SPP branch just described, a series of guided-mode branches, both above and below ω_{pb} , for which the amplitude H_y oscillates below the surface before decaying exponentially. The SPP bound to $\epsilon_R = 0$ may be thought of as the fundamental mode of this series.

For accumulation layers there may be two branches to the dispersion. The one at lower frequencies, which is always seen, begins for $\omega \ll \omega_{pb}$ by following the light line. At frequencies $\omega \gtrsim \omega_{pb}$ it departs from the light line and rises above the homogeneous sample dispersion to go asymptotically to $\omega_{ps}[\epsilon_\infty/(\epsilon_\infty + \epsilon_2)]^{1/2}$. This branch may lie higher than ω_{pb} since $\omega_{ps} > \omega_{pb}$ for this case. The second branch, which we have seen for $\omega_{pb}d/c \gtrsim 0.1$, generally lies above the first, for large ϵ_∞ occupying the corner formed by the intersection of the light line and the line $k_x = (\omega/c)[\epsilon_s(\omega)]^{1/2}$. For the accumulation-layer case when $\omega < \omega_{pb}$, so that $\epsilon < 0$ throughout the sample, the magnetic field behaves much like that of the usual SPP, although, in contrast to the depletion-layer case, the initial decay is more rapid than exponential. When $\omega_{ps} > \omega > \omega_{pb}$, branch I, and branch II also if it exists, has an extremum where $\epsilon_R = 0$. For branch I this point is a minimum, for II a maximum.

We have compared our results with two sets of data on InSb dispersion at room temperature. For the first set the SPP's were introduced by means of a grating ruled on the surface while in the second set a prism was used. For both sets the data fall below the dispersion for a sample homogeneous to the interface, indicating the presence of a depletion layer. By application of our theory to the experimental results, the depletion layer d was to be ~ 350 – 400 Å for the ruled samples, $\lesssim 60$ Å for the others, which is not unreasonable for an undisturbed surface.

Much more could be learned about surface layers by measuring SPP dispersion at lower temperatures and for large-gap semiconductors, where the d 's are larger. The experiments could be made to yield information about ω_{ps} as well as d if they were

carried to much larger k_x values. As indicated earlier, with holographic techniques it is possible to make photoresist gratings with periods smaller by a factor 50 than the smallest spacing used in Ref. 1. Interesting information could also be obtained by observing the effect on the dispersion of introducing electric fields, ambients or particular surface treatments to affect ω_{ps} .

APPENDIX A: INTEGRATION CONSTANT g

The integration constant g in the v solution is given by g_n , defined in (4.3), as $n \rightarrow \infty$. We derive here the approximate formula (4.5) to facilitate its computation. Substituting (3.16) and (3.17) into (4.3), we can arrange the result to give

$$g_n = g_{n-2} + (g_{n-1} - g_{n-2}) \{1 - qf_{n-1}[(n-1)(n-2) + \alpha(2n-3)]^{-1}\}^{-1} - \frac{1}{2}(q + \alpha^2)(2n-3 + 2\alpha)[(n-1)(n-2) + \alpha(2n-3) - qf_{n-1}]^{-1} + (q + \alpha^2)(n+1)[n(n-2)]^{-1}, \quad (\text{A1})$$

with

$$f_n = a_{n-1}/a_n. \quad (\text{A2})$$

Let the difference between two successive g_n 's be denoted by

$$h_n = g_n - g_{n-1}. \quad (\text{A3})$$

Then (A1) can be transformed into

$$h_n = [(n-1)(n-2) + \alpha(2n-3) - qf_{n-1}]^{-1} \{qh_{n-1}f_{n-1} + \frac{1}{2}(q + \alpha^2)[n(n-2)]^{-1}[(n-2)^2(2\alpha-1) + 2(n-1)(\alpha - qf_{n-1})]\}. \quad (\text{A4})$$

For large n , we find that

$$\lim_{n \rightarrow \infty} f_n = -1, \quad (\text{A5})$$

$$\lim_{n \rightarrow \infty} h_n = (q + \alpha^2)(2\alpha - 1)/(2n^2). \quad (\text{A6})$$

Because of (A6), $(g - g_n)$ vanishes rather slowly, according to n^{-1} , for large n . If the first two highest-order terms are kept, (A4) becomes

$$\lim_{n \rightarrow \infty} h_n = (q + \alpha^2)(2n^2)^{-1} [2\alpha - 1 - n^{-1}(1 - 6\alpha + 4\alpha^2 - 2q)]. \quad (\text{A7})$$

Returning to (A3), we may write

$$g = g_N + \sum_{n=N+1}^{\infty} h_n. \quad (\text{A8})$$

The substitution of (A7) into (A8) then yields (4.5). The two series in (4.5), which are related to the Riemann ζ function, converge rather quickly.

*Now at International Materials Research, 2950 Scott Blvd., Santa Clara, Calif. 95050.

¹N. Marschall, B. Fischer, and H. J. Queisser, *Phys. Rev. Lett.* **27**, 95 (1971); A. Hartstein and E. Burstein, *Solid State Commun.* **14**, 1223 (1974).

²W. E. Anderson, R. W. Alexander, and R. J. Bell, *Phys. Rev. Lett.* **27**, 1057 (1971).

³B. Fischer, N. Marschall, and H. J. Queisser, *Surf. Sci.* **34**, 50 (1973).

⁴R. F. Wallis, J. J. Brion, E. Burstein, and A. Hartstein, *Proceedings of the Eleventh International Conference on the Physics of Semiconductors* (PWN-Polish Scientific, Warsaw, 1972), p. 1448.

⁵S. L. Cunningham, A. A. Maradudin, and R. F. Wallis, *Phys. Rev. B* **10**, 3342 (1974).

⁶S. A. Rice, D. Guidotti, H. L. Lemberg, W. C. Murphy, and A. N. Bloch, in *Advances in Chemical Physics*, edited by I. Prigogine and S. A. Rice (Wiley, New York, 1974), Vol. XXVII.

⁷D. Guidotti, S. A. Rice, and H. L. Lemberg, *Solid State Commun.* **15**, 113 (1974).

⁸E. M. Conwell, *Phys. Rev. B* **11**, 1508 (1975).

⁹E. M. Conwell (unpublished).

¹⁰E. M. Conwell, *Solid State Commun.* **14**, 915 (1974).

¹¹See, for example, F. Seitz, *Modern Theory of Solids* (McGraw-Hill, New York, 1940).

¹²E. M. Conwell and C. C. Kao, *Optics Commun.*, **17**, 98 (1976).

¹³See, for example, L. D. Landau and E. M. Lifshitz, *Electrodynamics of Continuous Media* (Pergamon, New York, 1960).

¹⁴See, for example, Piaggio, *Differential Equations* (Bell, London, 1920).

¹⁵Strictly speaking, an additional boundary condition is needed at the surface for a conducting medium, as pointed out by F. Sauter, *Z. Phys.* **203**, 488 (1967). The error due to neglecting this could be significant when $\epsilon_I \gtrsim \epsilon_R$. This could give rise to a significant error in the dispersion when ϵ_R vanishes close to the surface. As will be seen, however, it would affect only a very small part of the dispersion curves, and only in the depletion-layer case.

¹⁶E. M. Conwell and C. C. Kao, *Solid State Commun.* 18, 1123 (1976).

¹⁷H. Welker and H. Weiss, in *Solid State Physics* edited by F. Seitz and D. Turnbull (Academic, New York, 1956), Vol. 3, p. 15.

¹⁸C. A. Mead and W. G. Spitzer, *Phys. Rev. Lett.* 10, 471 (1963).

¹⁹This calculation is carried out by CMW, who obtain 300 Å with the figures valid for 77 °K, the difference being presumably due to their use of a smaller value for m^* .

²⁰C. C. Kao and E. M. Conwell (unpublished).

²¹See, for example, W-T Tsang and S. Wang, *Appl. Phys. Lett.* 24, 196 (1974).